Materials Science-Poland, Vol. 25, No. 1, 2007

The solidification of CuCr alloys under various cooling rates

Y. WANG[1, 2*], X. SONG[1], Z. SUN[1], X. ZHOU[1], J. GUO[1]

[1]School of Science, Xi'an Jiaotong University, Xi'an 710049, P. R. China

[2]Institute of Materials Science and Engineering, Taiyuan Science and Technology University, Taiyuan 030024. P. R. China

The paper focuses on the solidification especially on the liquid phase separation of Cu–35 at. % Cr alloys under various cooling rates. When the solidification temperature is below the liquidus and above the spinodal temperature, solidification runs normally, with the growth of primary Cr-rich dendrites. When the solidification temperature is below the spinodal temperature, liquid phase separation should occur through the solidification process and the primary Cr-rich phase has a special nodular structure under an appropriate cooling rate. Large Cr-rich particles obtained from liquid phase separation can grow by absorbing smaller ones via the transfer of matter. Furthermore, some particles collide with each other, mutually losing surface energy by joining to form a single particle. The size of the Cr-rich particles obtained from liquid phase separation decreases with increasing cooling rate. Using thermodynamic calculations and referring to literature data, the viewpoints on liquid phase separation are systematized and applied to the CuCr system. Liquid phase separation in an undercooled liquid is not advantageous in refining the microstructure of alloys and should be restricted.

Key words: *solidification; liquid phase separation; CuCr alloy; melt spinning; microstructure*

1. Introduction

Liquid phase separation in the solidification process will occur in some systems with a stable or metastable miscibility gap, denoted in their diagrams under a large undercooling. The liquid phase separation of Cu–Co, Cu–Fe, and Cu–Co–Fe alloys has been described in previous papers [1–10]. The CuCr alloy is also a binary system having a flat liquidus (20~75 at. % Cr), with a dashed line for the miscibility gap and a dashed line for the spinodal in its diagram. Its liquid phase separation has been elucidated only in theory on the CuCr diagram [11–13].

*Corresponding author, e-mail: Wyheyj@163.com

The electromagnetic levitation and fluxing techniques are generally used in research work on liquid phase separation. Since the difference in the melting points of Cu and Cr is very large and Cr is still in solid state when the Cu liquid starts to drop, the electromagnetic levitation technique cannot be used to study CuCr alloys. There are some consuming reactions between CuCr alloys and slag glass, therefore the fluxing technique also cannot be used. Melt spinning is a common method for rapid solidification nowadays. By controlling the rotary speed of the cooling roller, various cooling rates can be produced. Finally, we succeeded in using the melt spinning technique for studying the liquid phase separation of CuCr alloys. This paper focuses on the solidification of Cu–35 at. % Cr alloys under various cooling rates.

2. Experimental

Pure (>99.95%) Cu and Cr were used to prepare the CuCr alloys by arc-melting. Some of the CuCr alloys were used as specimens with a lower cooling rate ($<10^3$ K/s)[14]. Subsequently, about 10g of the CuCr alloys were inserted into quartz tubes. When they were heated by high frequency induction to the required temperature, a ribbon was prepared by liquid quenching on a single roller melt spinning under the pressure of 0.5 atm Ar gas. The velocities of the cooling roller were 0.8 m/s and 33 m/s, and the corresponding calculated ribbon cooling rates were about 10^4 K/s and 10^6 K/s, respectively [15]. The dimensions (width×thickness) of the prepared ribbons were about 5 mm×800 μm and 3 mm×40 μm. The maximum undercooling of the 3 mm×40 μm ribbons was about 400–450 K [16, 17].

The microstructures of the samples were analyzed with an optical JSM 6460 scanning electron microscope (SEM) equipped with an energy dispersive spectrometer (EDS), and with a Hitachi H-800 transmission electron microscope (TEM). The foil specimen for the TEM was prepared by a twin-jet thinning device.

3. Results

3.1. Solidification of Cu–35 at. % Cr ingots at a cooling rate below 10^3 K/s

The microstructure of arc-melted Cu–35 at. % Cr ingots observed by SEM is shown in Fig. 1. The solidification of the ingots runs normally with the growth of primary Cr-rich dendrites (dark phase). Since the direction of dendritic growth is different, the dendrite arrowed in Fig. 1 is in the typical dendritic morphology, while some sections of dendrite look like snatchy structures. The entire sample was filled with this dendritic morphology. The Cu-rich phase (bright) was formed through an eutectic reaction.

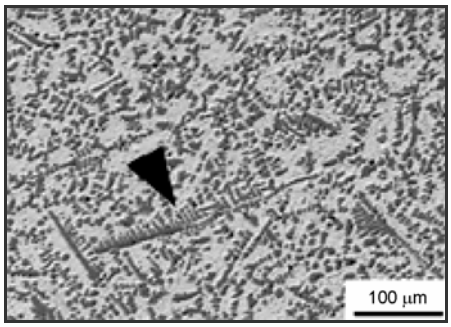

Fig. 1. The microstructure of arc-melted Cu –35 at. % Cr alloys observed by SEM. The arrow in the figure notes the primary Cr-rich dendrite. Etched with 5% HNO_3 + 95% C_2H_5OH

3.2. Solidification of CuCr ribbons at a cooling rate of about 10^4 K/s

In this part, ribbons about 5 mm wide and 800 μm thick were used as samples. There are many nodular particles in zone I oriented vertically, denoted by the arrow in Fig. 2a. The microstructure of zone I is shown in Fig. 2b and consists of large and nodular Cr-rich particles. Some particles are connected. The microstructure of zone II near the cooling surface in Fig. 2c consists of very small nodular Cr-rich particles. The microstructure of zone III near the free surface in Fig. 2d consists of Cr-rich dendrites.

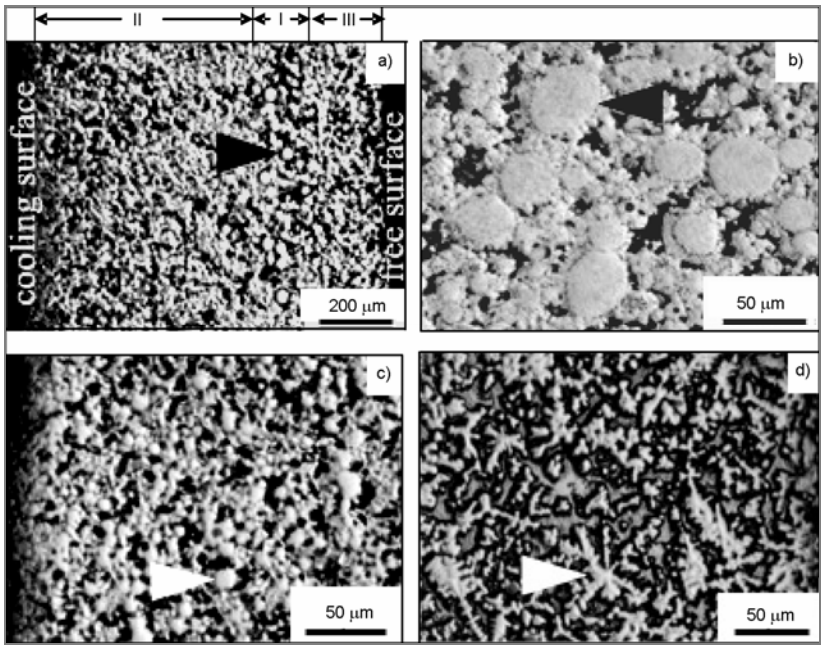

Fig. 2. The microstructures of melt spun Cu–35 at. % Cr ribbon at a cooling rate of about 10^4 K/s, observed by optical microscope: a) the cross section of the ribbon; b) zone I depicted by the arrow in Fig. 2a; c) zone II near the cooling surface; d) zone III near the free surface. The arrows in the Figure denote the Cr-rich particles obtained from liquid phase separation, except the arrow in Fig. 3d, which points to a Cr-rich dendrite. Etched with 80% $NH_3{\cdot}H_2O$ + 10% HCl + 10% Fe_2O_3

The change in the microstructures in melt spun Cu–35 at. % Cr ribbon is due to the change in the cooling rate or undercooling along the thickness of the ribbon. The higher the cooling rate, the smaller is the size of the primary Cr-rich phase. In contrast to Fig. 1, the microstructure of Cu–35 at. % Cr alloys was refined with increasing cooling rate. The larger nodular particle exists in zone I with a lower cooling rate.

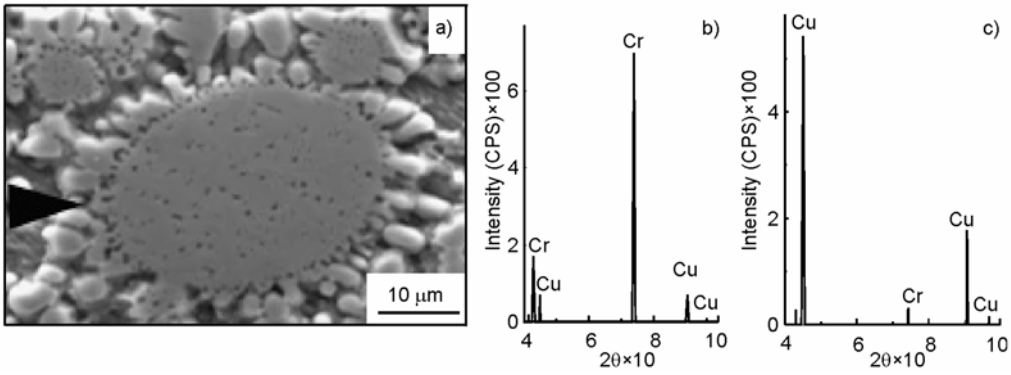

Fig. 3. The microstructure formed by liquid phase separation in a melt spun Cu–35 at. % Cr ribbon at a cooling rate of about 10^4 K/s, observed by SEM (a); X-ray diffraction diagrams of the gray phase in the Cr-rich particle (b); X-ray diffraction diagrams of the dark phase in Cr-rich particle (c); etched with 80% $NH_3{\cdot}H_2O$ + 10% HCl + 10% Fe_2O_3

Using SEM, the Cr-rich particle pointed out by the arrow in Fig. 2b was further studied and presented in Fig. 3a. Around its surface, there are many smaller Cr-rich particles that have an amalgamating tendency towards it. The large Cr-rich particle can grow by absorbing smaller ones via the transfer of matter. Furthermore, some particles collide with each other, mutually losing surface energy by joining to form a single particle [3]. Inside the particle, there is another phase (dark) besides the gray phase. According to EDS analysis (Figs. 3b, c), the gray phase is Cr-rich phase and the dark phase is Cu-rich. Robinson et al. [3] also observed a Cu-rich phase inside the Co particle obtained from liquid phase separation probably originating from liquid phase separation process. The behaviour of liquid phase separation in the CuCr system at a high cooling rate was confirmed experimentally.

3.3. Solidification of Cu–35 at. % Cr ribbons at a cooling rate of about 10^6 K/s

The microstructure of melt spun $CuCr_{35}$ ribbon 3 mm wide and 40 μm thick observed by TEM is shown in Fig. 4a. From their morphologies, one cannot tell whether these primary Cr-rich particles originate from liquid phase separation or from the general solidification process. This will be analyzed later in the discussion. The diameters of the primary Cr-rich particles were decreased to below 300 nm by increasing the cooling rate.

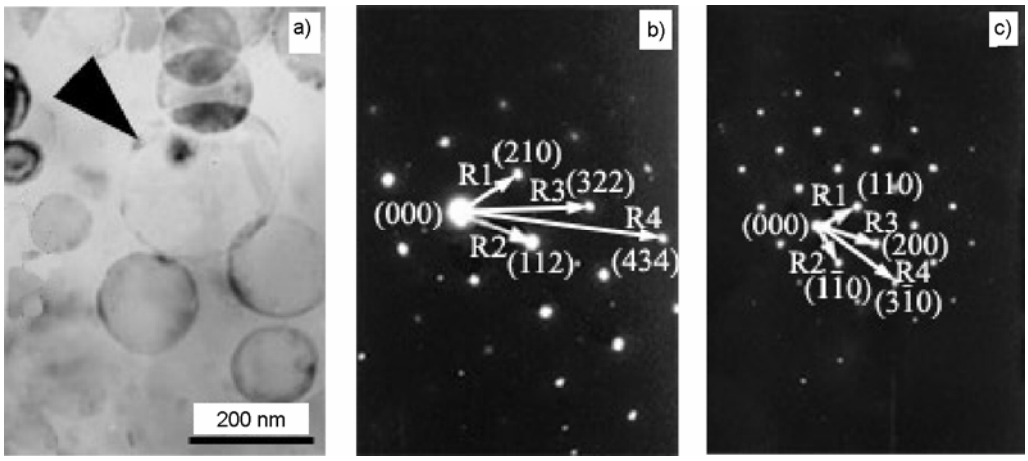

Fig. 4. Microstructure of melt spun Cu–35 at. % Cr ribbon at the cooling rate of about 10^6 K/s, observed by TEM (a); the arrow in the Figure points to a Cr-rich particle from liquid phase separation: electron diffraction pattern of the matrix (b); electron diffraction pattern of Cr-rich particle (c)

Figure 4b shows the electron diffraction pattern of the matrix, and the results of the analysis are given in Table; R_i is the distance between two points, N is the integer of $3R_i^2/R_1^2$, (hkl) is the index of the crystal face, $[uvw]$ is the zone axis, $d = K/R$ is the calculated interplanar spacing, K is the camera constant, $d_{\mathrm{Cu,standard}}$ is the interplanar spacing of Cu in a standard, $\angle R_1R_2$ is the angle between $(h_1k_1l_1)$ and $(h_2k_2l_2)$. As a result, we know that the matrix is *FCC* Cu. Figure 4c shows the electron diffraction pattern of the primary Cr-rich particle. The results of the analysis are shown in Table 2. Therefore, we know that the primary Cr-rich particle is *BCC* Cr.

Table 1. The results of the analysis for the electron diffraction pattern of the matrix in Fig. 4b*

R_i (mm)	$3R_i^2/R_1^2$	N	hkl	uvw	d = (Å)	$d_{\mathrm{Cu,standard}}$ (Å)
R_1 = 14.3	3.00	3	210	1$\bar{4}$1	1.6071	1.6168
R_2 = 16.3	3.90	4	112		1.4103	1.4759
R_3 = 27.5	11.05	11	322		0.8375	0.8768
R_4 = 37.0	27.01	27	434		0.5356	0.5646

*K = 23.03 mm·Å, $\angle R_1R_2$ = 57° (standard: 56.79°).

Table 2. The results of the analysis for the electron diffraction pattern of the Cr-rich particle in Fig. 4c*

R_i (mm)	$3R_i^2/R_1^2$	N	hkl	uvw	$d = K/R$ (Å)	$d_{\mathrm{Cu,standard}}$ (Å)
R_1 = 9	2.00	2	110	$\bar{2}0\bar{2}$	2.0106	2.0269
R_2 = 9	2.00	2	1$\bar{1}$0		2.0106	2.0269
R_3 = 13	4.17	4	200		1.3919	1.4332
R_4 = 20	9.88	10	3$\bar{1}$0		0.9048	0.9064

*K = 18.11 mm·Å, $\angle R_1R_2$ = 90° (standard: 90°).

4. Discussion

Figure 5 shows the Cu–Cr phase diagram [11–13] and mixing Gibbs energy (G_m) in undercooled CuCr liquid at 1500 K as calculated by us. According to the microstructure in Fig. 1 and considering the cooling rate in the solidification process, the solidification temperature of Cu–35 at. % Cr ingots should be below its liquidus and above its spinodal in Fig. 5a. The solidification in Fig. 5a can be expressed as: B (undercooled liquid) → A (liquid) + C (Cr solid), which runs normally. In this case, liquid phase separation does not occur during solidification.

Before discussing how the microstructures in Figs. 2, 3 were formed, the theory of liquid phase separation should be analysed. The mixing Gibbs energy of binary alloy systems can be expressed as:

$$G_m = RT(X_i \ln X_i + X_j \ln X_j) + \Omega_{ij} X_i X_j \tag{1}$$

where X_i is the mol fraction of a component i, Ω_{ij} is the interaction parameter between components i and j, R is the gas constant, and T is temperature in Kelvins.

Using the published data in [11], G_m of the undercooled liquid of the CuCr system at 1500 K was calculated from Eq. (1) as an example. The result is shown in Fig. 5b. Comparing Fig. 5a and Fig. 5b, the dashed line of the miscibility gap was calculated from the equality

$$\frac{\partial G_m}{\partial X_{\mathrm{Cr}}} = 0$$

The miscibility gap dashed line [18] corresponds to the minimum of the G_m value of the undercooled liquid. Undercooled liquids with compositions between points K and P in Fig. 5b tend to demix into a Cu-rich liquid (point K) and a Cr-rich liquid (point P), thus G_m of system will go down. The dashed line of the spinodal was calculated from the equality:

$$\frac{\partial^2 G_m}{\partial X_{\mathrm{Cr}}^2} = 0$$

Undercooled liquids with compositions between points M and O in Fig. 5b (inside the spinodal in Fig. 5a will start to demix spontaneously without nucleation. Undercooled liquids with compositions between points K, M, O, and P in Fig. 5b (outside the spinodal and inside the miscibility gap in Fig. 5a cannot demix at 1500 K, and will demix at a lower temperature.

After demixing, the solidification of the Cu-rich and Cr-rich liquids is inexplicit in theory. According to [3], there is a viewpoint that *once separated, the two liquids have different undercoolings with regard to their respective liquidus temperature*. [...] *As a result, L1 could solidify first according to the nucleation thermodynamics* … This implies that we can treat the two separated liquids within the general solidification theory after demixing.

Therefore, the solidification of the Cu-rich and Cr-rich liquids can be expressed as:

$$\text{I (Cr-rich liquid)} \rightarrow \text{D(liquid)} + \text{J(Cr solid)}$$

$$\text{E (Cu-rich liquid)} \rightarrow \text{D(liquid)} + \text{J(Cr solid)}$$

as seen in Fig. 5a. Robinson et al. [3], however, pointed out that the former transition is easier than the latter.

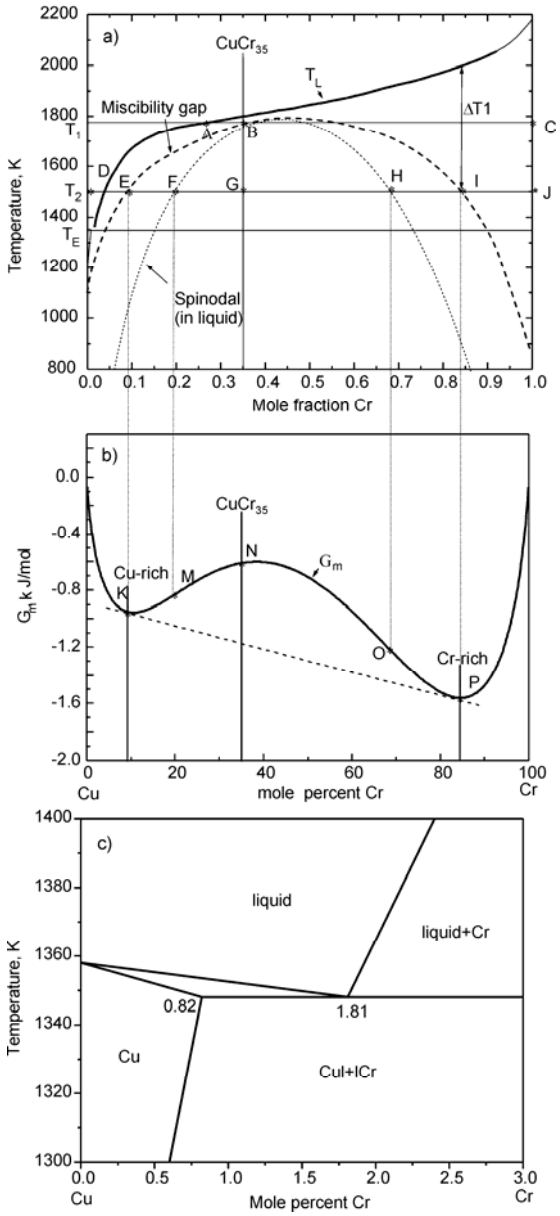

Fig. 5. Cu–Cr phase diagram [11] (a), mixing Gibbs energy of CuCr liquid at 1500 K (b), Cu–Cr phase diagram at the Cu-rich side (c)

Although the undercooling of the separated Cr-rich liquid is larger than that of the homogeneous $CuCr_{35}$ liquid at temperature T_2 in Fig. 5a, the size of the Cr solid phase in the Cr-rich liquid zone cannot be decreased by this factor because the growth of the Cr solid phase occurs in an undercooled liquid of about Cu–84% Cr, in which there are many Cr atoms. Therefore, the liquid phase separation in the undercooled liquid is not advantageous in refining the microstructure of alloys and should be restricted.

Considering the microstructures in Figs. 2, 3 and the cooling rate of the solidification process, the solidification temperature of zone II near the cooling surface and zone I pointed to by the arrow in Fig. 2a should be below its spinodal temperature. In the solidification processes of these two zones, liquid phase separation should occur. The solidification temperature of zone III near the free surface, however, should be above its spinodal temperature, as its solidification still runs normally.

Because undercooling increases as the cooling rate is increased, the solidification temperature at a cooling rate of about 10^6 K/s should be between the spinodal and the eutectic temperatures. According to the liquid phase separation theory presented above, the primary Cr-rich particles in Fig. 4a should originate from liquid phase separation.

5. Conclusions

When the solidification temperature is below its liquidus and above its spinodal, the solidification of Cu–35 at. % Cr alloys runs normally, with a growth of primary Cr-rich dendrites and the primary Cr-rich dendrites larger than 200 μm. After increasing the cooling rate to about 10^4 K/s, the solidification temperature of most of the cross section of melt spun Cu–35 at. % Cr ribbon, except zone III, should be below its spinodal temperature, and liquid phase separation should occur during the solidification process. The diameter of the larger Cr-rich particles is about 20 μm. The large Cr-rich particles can grow by absorbing smaller ones via the transfer of matter. Furthermore, some particles collide with each other, mutually losing surface energy by joining to form a single particle. After further increasing the cooling rate to about 10^6 K/s, the diameter of larger Cr-rich particles obtained from liquid phase separation is decreased to about 250 nm. The size of the Cr-rich particles obtained from liquid phase separation will decrease as the cooling rate is increased.

Using thermodynamic calculations and referring to other papers, the viewpoints on liquid phase separation are systematized and applied to the CuCr system. Liquid phase separation in undercooled liquid is not advantageous in refining the microstructure of alloys and should be restricted.

Acknowledgements

The authors would like to thank the National Science Foundation of China (grant No. 50371066) for their financial support.

References

[1] ELDER S.P., MUNITZ A., ABBASCHIAN G.J., Mater. Sci. Forum, 50 (1989), 137.
[2] MUNITZ A., J. Mater. Sci., 33 (1998), 3639.
[3] ROBINSON M.B., LI D., RATHZ T.J., WILLIAMS G., J. Mater. Sci., 34 (1999), 3747.
[4] SONG X., MAHON S.W., COCHRANE HOWSON R.F., Mater. Lett., 31 (1997), 261.
[5] PEREPECZKO J.H., SHIAHARA Y., PAIK J.S., FLEMINGS M.C., [in:] *Rapid Solidification Processing, Principles and Technologies III*, NBS, Gaithersburg, MD, (1982), 28.
[6] CHONGDE C., XIAOYU L., BINGBO W., Acta Metall. Sin., 5 (1998), 490.
[7] MUNITZ A., ELDER-RANDALL S.P., ABBASCHIAN R., Metall. Trans. A, 23 (1992), 1817.
[8] ABBASCHIAN G.J., FLEMINGS M.C., Metall. Trans. A, 14 (1983), 1147.
[9] XIAOYU L., CHONGDE C., BINGBO W., Acta Photon. Sin., Z3 (1998), 121.
[10] LI D., ROBINSON M.B., RATHZ T.J., J. Phase Equil., 21 (2000), 136.
[11] JACOB K.T., PRIYA S., WASEDA Y., Metall. Z., 91 (2000), 594.
[12] ZENG K., HÄMÄLÄINEN M., Calphad, 19 (1995), 93.
[13] MICHAELSEN C., GENTE C., BORMANN R., J. Mater. Res. 12 (1997), 1463.
[14] GRANT N.J., J. Metals, 1 (1983), 20.
[15] YOUHONG W., ZHANBO S., XIAOPING S., Chinese J. Nonferrous Met., 15 (2005), 1045.
[16] MASLOV V.V., NOSENKO V.K., J. Mater. Sci., 37 (2002), 4663.
[17] LIU F., YANG G., GUO X., J. Mater. Sci., 36 (2001), 3607.
[18] DEHOFF R.T., *Thermodynamics in Materials Science*, McGraw-Hill, Columbus, 1993, p. 255–260.

Received 19 June 2006
Revised 5 July 2006